

Origin of the second length scale found above T_N in UO_2

G. M. Watson

Department of Physics, Brookhaven National Laboratory, Upton, New York 11973-5000

B. D. Gaulin

Department of Physics and Astronomy, McMaster University, Hamilton, Ontario, Canada L8S 4M1

Doon Gibbs, T. R. Thurston, P. J. Simpson,* and S. M. Shapiro

Department of Physics, Brookhaven National Laboratory, Upton, New York 11973-5000

G. H. Lander and Hj. Matzke

European Commission, Joint Research Center, Institute for Transuranium Elements, Postfach 2340, D-76125 Karlsruhe, Germany

S. Wang and M. Dudley

Department of Materials Science and Engineering, State University of New York at Stony Brook, Stony Brook, New York 11794-2275

(Received 26 May 1995)

We present the results of x-ray- and neutron-scattering studies of the temperature dependence of the magnetic scattering exhibited by the type-I, triple- Q antiferromagnet UO_2 . Our neutron-scattering results are consistent with those of earlier studies, including the observation of short-ranged magnetic correlations at temperatures near and above T_N . However, it is found by x-ray diffraction that a second, longer length scale is induced near T_N when the near-surface volume of the sample is mechanically roughened. The longitudinal and transverse widths of the additional scattering increase continuously with increasing temperature above T_N , similar to that which has been observed near the magnetic ordering transitions of Ho, Tb, and NpAs and near the tetragonal-to-cubic transitions of various perovskites. Another unusual feature of the present results for UO_2 involves the apparent shift with temperature of the magnetic scattering along the surface normal direction at the (1,1,0) reflection, but not at the (2,1,0) reflection. To our knowledge, this is the first observation of a second length scale near a first-order transition.

I. INTRODUCTION

In the mid-1980s, Andrews and colleagues¹⁻³ carried out comprehensive, high-resolution x-ray-scattering studies of the tetragonal-to-cubic structural transformation of the perovskite SrTiO_3 . Surprisingly, they reported the observation of two length scales among the critical fluctuations near T_C instead of one, as would be expected in an ideal system. The two length scales differed in magnitude by nearly a factor of ten. Similar results were subsequently discovered in the critical behavior of other perovskites, including RbCaF_3 (Refs. 4 and 5) and KMnF_3 .⁶ On the basis of the measured temperature dependence, the shorter length scale was identified with the “normal” critical scattering, as described by the soft-mode theory of displacive phase transformations. The existence of the second, longer length scale could not be explained by the conventional theory of critical phenomena, and indeed its origin remains unclear today.

The key idea employed to understand the origin of the second length scale has been to focus on the effects of disorder on otherwise ideal phase transitions. Imry and Wortis,⁷ in particular, considered the effect of random defects on first-order transitions. They showed that it is possible for local fluctuations to occur from one phase into the other in domains centered on defect sites, provided that the free energy gained thereby is balanced by the cost of producing the domain wall. One imagines there being a distribution of local

transition temperatures T_C across the sample, with the respective length scales of the fluctuations controlled by the free-energy differences between the two phases. While qualitatively appealing, it has been difficult to adapt these ideas to specific experimental systems. Moreover, it has not been straightforward to produce and characterize samples with well-known defect distributions, or, even better, to produce samples in which the strain can be easily tuned.

More recently, two-length-scale line shapes have been observed in x-ray- and neutron-scattering studies of magnetic ordering transformations in the rare earths Ho (Refs. 8 and 9) and Tb,^{10,11} in NpAs,¹² UAs,¹³ and others. Various qualitative features of the temperature dependence of the second length scale, including its apparent divergence near T_N and the anomalous exponents of the correlation lengths, are similar to those of the perovskites—and motivate the idea that the two phenomena are related. In this regard, Axe¹⁴ has noted that magnetoelastically induced, random strains may also couple quadratically to the order parameter in the free energy, which makes the analogy to the perovskites physically plausible. An intriguing feature of the problem, which has been clarified in the more recent experiments, is the predominant localization of the additional component in the volume near the sample surface. Specifically, it has been found that x-ray-scattering experiments are especially sensitive to the sharp component directly as a result of the typically shallow penetration depths ($\sim 1 \mu\text{m}$ at 8 keV in rare earths) and

the very high q resolution.^{8,9} Furthermore, small-angle neutron-diffraction experiments on Tb (Refs. 10 and 11) have isolated the sharp component within the near-surface volume, although over a surprisingly large distance of 0.3 mm.

These results have raised the possibility that the longer-length-scale fluctuations are intrinsic to interfaces. It is well known, for example, that the relief of stress associated with an ideally terminated surface in vacuum can lead to surface reconstruction.¹⁵ The corresponding modification of near-surface critical behavior has been discussed previously in many contexts (see, for example, Ref. 16), including in application to the two-length-scale problem of the perovskites.^{1-6,17} In this regard, Cowley¹⁸ has considered the possibility of spontaneous surface strains which enter the free energy in fourth order, thereby producing a second length scale. Although we cannot rule out the possibility of intrinsic surface strains in the present experiments, our results suggest instead that the sharp component is correlated with the presence of strain fields, which may exist either in the bulk or near the surface, but which commonly reside in the near-surface volume as a result of mechanical or chemical polishing. Along these lines, intriguing results have been reported for thin slices of SrTiO₃ single crystal, in which only a sharp component is found by neutron scattering.¹⁹

In this paper, we report x-ray- and neutron-scattering studies of the temperature dependence of the magnetic scattering of the antiferromagnet UO₂. In contrast to other systems exhibiting two length scales, the magnetic structure of UO₂ is triple Q and the magnetic ordering transition is first order. From earlier x-ray magnetic-scattering experiments,²⁰ UO₂ is well known to produce large magnetic signals for incident x-ray energies tuned near the M_{IV} absorption edge (3.728 keV). At these energies, the $(1/e)$ absorption length is only about 1200 Å, making these experiments especially sensitive to the near-surface volume. For this reason, extended fine polishing and annealing of the surface was undertaken to produce as nearly perfect a sample as possible (stopping short of *in situ* preparation and characterization). Subsequently, one-third of the sample was mechanically roughened, in order to introduce strains at the surface. Scanning electron microscopy, x-ray topography, positron annihilation, Rutherford backscattering, and x-ray diffraction techniques were all used to characterize the near-surface structure and morphology of both sides of the sample. The damaged region was found to extend about 0.5 μm into the sample, and to possess a mosaic width nearly twice that of the as-prepared side, with weaker integrated intensities and additional scattering in the wings. We believe this is consistent with a significant, probably random, strain.

The main result of the present work is the observation by x-ray diffraction of a second, sharp component of the magnetic scattering above T_N on the mechanically roughened side of the sample, which is absent on the as-prepared side. In contrast, our neutron-diffraction studies revealed only a broad component, consistent with normal short-ranged fluctuations and with earlier neutron-scattering studies. The additional, sharp component is about ten times narrower than the broad component and increases in width with increasing temperature. There is, in addition, an apparent shift in position of the magnetic scattering at the (1,1,0) reflection along

the surface normal direction with temperature above T_N . We believe this latter effect probably reflects the change in d spacing of the lattice domains supporting magnetic correlations. However, a similar shift was not observed at the (2,1,0) reflection, which may raise the possibility that there are two kinds of magnetic domain in the near-surface region.

Although many questions remain unresolved, our results suggest that the second length scale observed in UO₂ is correlated with the residual strain in the near-surface volume, left after mechanical roughening. On this basis, we further suggest that the presence of a second, sharp component among the critical fluctuations of both magnetic and structural phase transitions most likely reflects the influence of random strain fields. Unfortunately, it has been impossible in the present experiments to characterize the detailed microscopic strain distribution at the surface. The physical mechanism which leads to the second component, therefore, remains unclear. Definitive conclusions still require more systematic studies with finer control of the strain distribution, such as has been possible in studies of random-field Ising systems.^{21,22} From the perspective of exploring model systems, however, these results illustrate the importance of sample growth and preparation, especially as high-resolution, synchrotron radiation techniques make probing large length scales routine. For temperatures very near T_N , even a small amount of disorder can significantly alter the phase behavior. Disentangling and understanding the effects of minute amounts of disorder from the intrinsic behavior near first-order and continuous phase transitions poses an interesting, but challenging, problem for third-generation synchrotron radiation experiments.

In Sec. II of the following we describe the details of the x-ray- and neutron-scattering experiments, including the characterization of the mechanically roughened and as-prepared sides of the sample. Our results are presented in Sec. III and a discussion in Sec. IV.

II. EXPERIMENTAL DETAILS

A. Magnetic structure of UO₂

UO₂ has the face-centered-cubic fluorite structure, with $a=5.47$ Å at room temperature. The Hund's rule ground state is 3H_4 with two $5f$ electrons on each U⁴⁺ ion. Below $T_N=30.2$ K, UO₂ forms a type-I, triple- Q antiferromagnet, consisting of ferromagnetic (0,0,1) planes stacked in alternating sequences (+-) along each of the simple cubic directions.²³⁻²⁵ All three modulation directions exist simultaneously within the magnetic unit cell. The allowed magnetic reflections are obtained by adding a [0,0,1]-type wave vector to any fcc-allowed charge reflection. This is illustrated in Fig. 1, where a reciprocal space map showing the allowed charge and magnetic Bragg reflections is shown. The magnetic scattering observed at (1,1,0) can be obtained by adding the magnetic modulation wave vector, $Q_M=(0,0,-1)$ to the (1,1,1) charge reflection. The component of the magnetic structure contributing to a given reflection lies in a plane perpendicular to the magnetic wave vector Q_M . For all temperatures below T_N , the magnetic structure is commensurate with the lattice. At T_N , the abrupt change in magnetic intensities measured by neutron scattering²³⁻²⁵ and anomalies in the elastic constants²⁶ have established that the magnetic or-

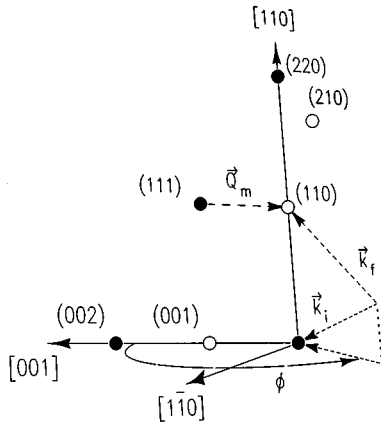


FIG. 1. Reciprocal space map showing allowed charge (filled circles) and magnetic (open circles) Bragg reflections. The dashed line shows the (110) magnetic reflection referred to the (111) charge reflection. The corresponding magnetic modulation wave vector Q_M is shown. Incident (k_i) and scattered (k_f) wave vectors are indicated by the dashed arrows. The azimuthal angle ϕ is defined by the (001) axis and the projection of k_i in the (001) \times (110) plane. Most of the experiments were performed with the azimuthal angle $\phi=68^\circ$. The surface-normal direction is along [1,1,0]. The choice of incident x-ray wavelength near the M_{IV} edge (3.728 keV) limits the range of accessible reciprocal space to reflections with momentum transfers less than about (2,2,0).

dering transformation is first order. It has also been shown that magnetic ordering occurs without detectable changes in the bulk lattice constants or observable thermal hysteresis of the magnetic intensities (the latter except within about 0.04 K of the Néel temperature²³). Broad magnetic scattering has been observed by neutron diffraction²⁷ over a temperature range of about 5 K above T_N ; it is characterized by magnetic correlation lengths of order 10 Å near T_N , and is typical of the magnetic fluctuations observed near first-order transitions.

B. Experimental setup

The x-ray-scattering experiments were performed on bending magnet beamline X22C at the National Synchrotron Light Source (NSLS) at Brookhaven National Laboratory. The incident beam was focused to a spot size of about 1 mm² using a toroidally bent, nickel-coated mirror, and monochromatized using a double-crystal Ge(111) monochromator. NaI scintillation counters were used to count the incident and scattered photons. All of the x-ray experiments were performed at an incident photon energy of 3.728 keV, which corresponds to the M_{IV} absorption edge of uranium. Special care was taken to minimize intensity losses due to air scattering and absorption by the Be and kapton windows of the beamline, as has been described in earlier work.²⁰ The sample was mounted in a closed-cycle He refrigerator with temperature stability of ~ 0.02 K over several hours, and the temperature was monitored using Si-diode thermometers.

The choice of incident wavelength follows from the existence of large, resonant enhancements of the magnetic signal which occur when the incident x-ray energy is tuned near the L or M absorption edges of the rare earths and actinides.^{12,20,28–34} As a result of these enhancements, it has

become possible to probe critical magnetic fluctuations with very high q resolution by x-ray scattering.^{8–13,35} The details of x-ray resonant processes are available in the literature.^{28–34} We summarize a few relevant facts in the following.

For uranium compounds, the largest enhancements observed to date occur at the M_{IV} and M_V absorption edges (the latter corresponding to an incident photon energy of 3.55 keV). At the M_{IV} edge, the dominant scattering involves electric dipole excitations, in which the incident photon promotes an electron from the filled $3d_{3/2}$ core to an empty $5f_{5/2}$ state. In the subsequent decay of the excited state, an elastically scattered photon may be emitted. The amplitude of the resonant cross section depends on the overlap of the ground and excited magnetic states allowed by the exclusion principle. This overlap is large at the M_{IV} absorption edges of the actinides, leading to magnetic intensities as great as 1% of the charge scattering intensities from the lattice.³¹

Earlier studies of a series of actinides,^{20,31} including UO_2 , have already established the basic x-ray resonant-diffraction characteristics of these materials. Large intensities, of order 1×10^5 /sec and greater (at typical NSLS beam currents of ~ 150 mA), have been reported for incident photon energies near the M_{IV} edge. Polarization analysis of the magnetic scattering has confirmed the mainly dipole character of the process. Fitting of the line shapes and intensities obtained at the M_{IV} and M_V edges was found to give results qualitatively consistent with the known electronic structures, provided crystal-field splittings were included for UO_2 .²⁰ Recently, the cross section for x-ray magnetic scattering has been expressed in terms of tensor operators of the orbital and spin magnetization densities.^{32–34} Under the assumption of spherical symmetry, the dipole magnetic scattering which occurs at the magnetic wave vector is predominantly proportional to a two-spin correlation function, entirely analogously to the cross section for neutron diffraction. In the following discussion, therefore, we assume that the intensities are proportional to the square of the magnetization density, just as for neutron scattering.

The neutron-scattering experiments were performed at the High Flux Beam Reactor on spectrometer H4M. The spectrometer was run in the energy-integrating double-axis mode with an incident neutron energy of 14.7 meV. The resolution in reciprocal space was determined by a series of collimators. For the configuration used, 20'-20'-sample-20'-open, the resulting resolution at the elastic position was 0.017 and 0.008 Å⁻¹ in the longitudinal and transverse directions, respectively. Cadmium foil was used to mask the as-prepared and roughened parts of the sample, respectively. As in the x-ray measurements, the sample was mounted in a closed-cycle He refrigerator. The temperature, measured using a Si diode, was stable to within 0.02 K over the several hours required to obtain a scan.

C. Surface preparation and characterization

The sample was cut from an oriented UO_2 single crystal to produce a (1,1,0) surface, about 20×5 mm² in area. The surface was polished first with a sequence of different emery papers, decreasing to a 600 mesh, and then by a series of diamond pastes, ranging from 25 to 0.25 μm grains. The latter procedure removes most of the mechanical surface

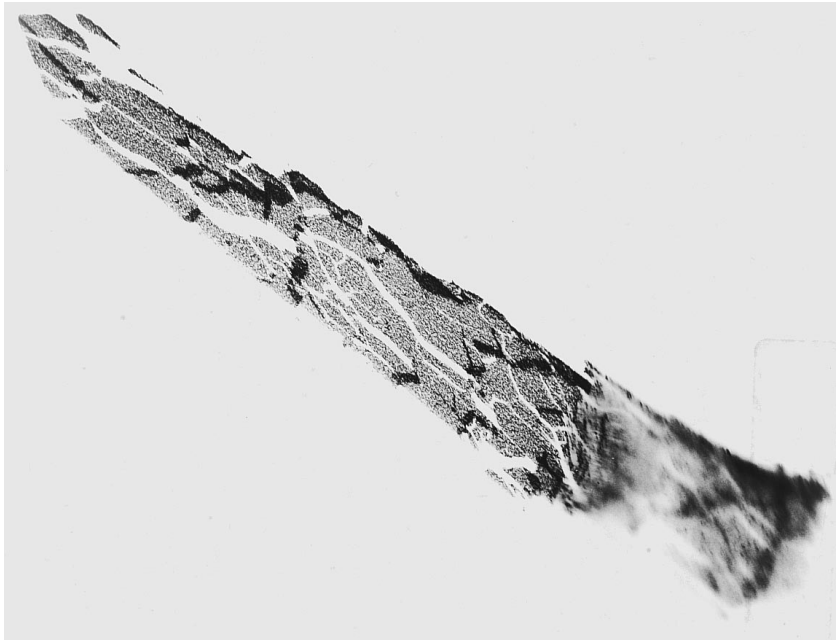


FIG. 2. X-ray topograph showing the entire sample (of dimensions $\sim 20 \times 5$ mm²). Well-resolved crystallites are visible on the upper two-thirds of the sample. The lower one-third was mechanically roughened, leading to its blurry appearance.

damage introduced by cutting. The remaining damage (at least within a $0.25 \mu\text{m}$ layer) was further reduced by annealing in an Ar/H₂ atmosphere at 1400°C for about one hour. Subsequent Rutherford backscattering/channeling experiments with 2 MeV He⁺ ions gave the minimum aligned yield of $\chi_{\text{min}}=0.02$. This corresponds to the value theoretically expected from thermal vibrations of the surface atoms.^{36,37}

About one-third of the sample surface was then mechanically roughened using sandpaper. The resulting damage is illustrated on the right-hand side of Fig. 2, which shows an x-ray topograph of the entire sample. The topograph was obtained using the (1,1,3) chemical reflection at an incident wavelength of 0.90 \AA on NSLS beamline X19. The incident angle to the surface was about 1° , corresponding to an x-ray penetration depth of $0.1 \mu\text{m}$. As may be seen, the left-hand side of the image shows a patchwork of well-resolved (1,1,0) crystallites, extending in some case up to 1 mm in length. In contrast, the right-hand side of the image is blurry, consistent with significant mechanical damage. A series of x-ray topographs taken of this sample has established that the damaged region extends about $0.3 \mu\text{m}$ into the surface, below which images from the right- and left-hand sides of the sample become qualitatively similar. It has not been possible, however, to identify simple, single-site defects by x-ray topography.

Scanning electron microscopy images of the as-prepared and mechanically roughened surfaces of the sample are shown on the left- and right-hand sides, respectively, of Fig. 3. The top panels correspond to low-resolution images (bar = $100 \mu\text{m}$) while the bottom panels correspond to a higher-resolution image (bar = $10 \mu\text{m}$). The principal features visible on the as-prepared side of the sample are $\sim 1 \mu\text{m}$ wide line scratches running along two different directions in the photograph. In addition, there are dark spots, which we believe correspond to inclusions, possibly of diamond particles. In contrast, the mechanically roughened side of the sample is significantly damaged on both 100 and $10 \mu\text{m}$ length scales, and shows a complex surface morphology.

Evidence of vacancy-type defects present on both sides of the sample has been obtained from variable-energy positron annihilation measurements.³⁸ In these experiments, positrons are implanted to a controlled depth and then diffuse until they either annihilate or become trapped by a defect. The annihilation environment is characterized by measuring the *width* of the 511 keV annihilation γ -ray line, which is Doppler broadened due to the momentum of the annihilating electron. Positrons trapped in open-volume defects have a reduced probability of annihilation with high-momentum core electrons, giving a *narrower* annihilation line. The line-width is parametrized simply by taking the fraction of the total counts occurring in a central region of the annihilation photopeak—the so-called “*S* parameter.” A modeling procedure is required to deconvolve the effects of the positron implantation profile, and subsequent thermal diffusion. This yields an approximate depth profile of defects. Figure 4 shows *S*-parameter data (lower panel) obtained from the as-prepared and mechanically roughened sides of the sample, together with the defect densities used to model the data (upper panel). While the defect densities and depth distributions given can only be estimates, two features of the data are clear and are independent of detailed numerical interpretation: (i) both sides of the sample contain high vacancy-type defect densities in the near-surface ($\sim 0.1 \mu\text{m}$) region, and (ii) these defects extend to a much greater depth ($\geq 0.6 \mu\text{m}$) on the mechanically roughened side of the sample.

Although the results of x-ray topography, scanning electron microscopy (SEM), and positron depth-profiling experiments are all qualitatively consistent with each other, and suggest that the defect density on the mechanically roughened side of the sample is considerably greater than on the as-prepared side, it should be emphasized that the damage is so great that these techniques have not permitted simple, quantitative conclusions to be drawn concerning the predominant defect type near the sample surface, nor about the strain profile.

Perhaps the most useful characterization of the structural perfection of the two sides of the sample is obtained from the

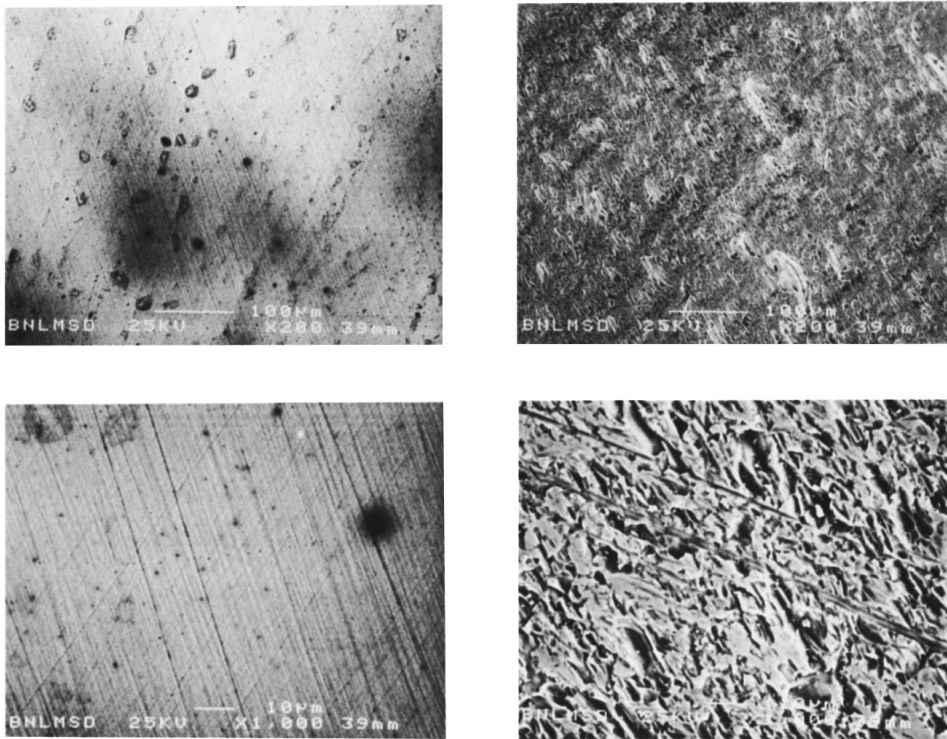


FIG. 3. Scanning electron microscopy images of the as-prepared (left) and mechanically roughened (right) sides of the sample. The white bar in the two upper photographs corresponds to $100\ \mu\text{m}$, while in the two lower photographs it corresponds to $10\ \mu\text{m}$.

x-ray-scattering profiles of the charge and magnetic scattering at the $(2,2,0)$ and $(1,1,0)$ reflections, respectively, in the magnetically ordered phase. Since these were obtained at an incident x-ray energy of $3.728\ \text{keV}$, they directly reflect the volume probed in the x-ray-scattering experiments. The upper and lower panels of Fig. 5 show the results of transverse

and longitudinal scans, respectively, taken through the $(2,2,0)$ charge scattering peak at $13\ \text{K}$. Open circles represent the data obtained on the mechanically roughened side of the sample, while solid lines represent the data obtained on the as-prepared side. The insets show the same data plotted with the amplitudes rescaled in order that the peak heights coincide. As may be seen, the profiles obtained on the roughened side are reduced in amplitude and broader than those obtained on the smooth side. The integrated intensities on the roughened side are also typically reduced relative to the as-prepared side, suggesting the partial loss of translational order of the lattice. The largest differences are apparent in the wings of the scattering, which extend more than $0.003\ \text{\AA}^{-1}$ around the peak on the roughened side, consistent with a distribution of domains with varying lattice constants.

The charge-scattering profiles were fitted to Lorentzian-squared and Lorentzian-three-halves line shapes on the as-prepared and roughened sides, respectively. These line shapes (and all following) were chosen for convenience of fitting; no particular significance is attached to their forms. The longitudinal full width at half maximum (FWHM) on the as-prepared side was found to be $0.0012\sqrt{2}a^* = 0.002\ \text{\AA}^{-1}$ and $0.0015\sqrt{2}a^* = 0.0024\ \text{\AA}^{-1}$ on the roughened side. Assuming that the longitudinal width of the as-prepared surface gives the instrumental resolution in these experiments, we infer a lattice correlation length of at least $1000\ \text{\AA}$ along the surface-normal direction. This length is comparable to the $(1/e)$ absorption depth (about $1200\ \text{\AA}$) at these incident x-ray energies. The corresponding correlation length on the damaged side appears comparable (or slightly smaller, $\sim 800\ \text{\AA}$) in the regions of the sample which support translational order. The mosaic widths were found to be $0.027(2)^\circ$ and $0.043(2)^\circ$ on the as-prepared and roughened sides of the sample, respectively. The additional width on the roughened side probably reflects either an increase in the relative orien-

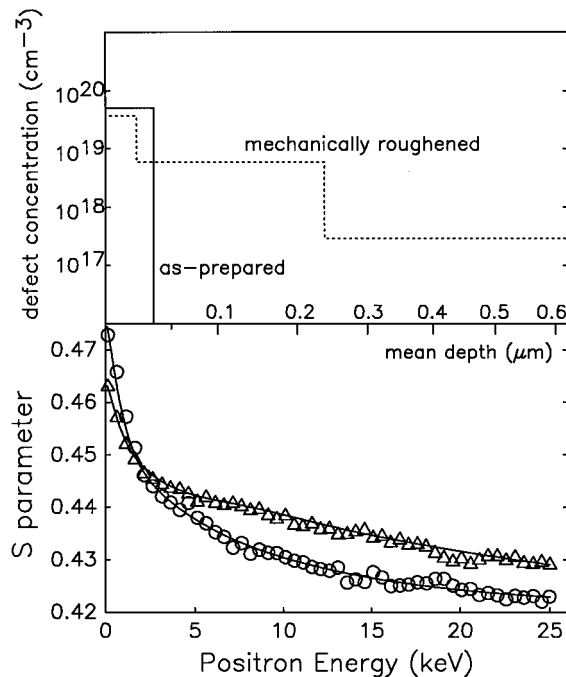


FIG. 4. Lower: S parameter versus positron energy for the as-prepared (open triangles) and mechanically roughened (open circles) sides of the sample, respectively. Upper: The inferred vacancy defect densities from the as-prepared and mechanically roughened sides.

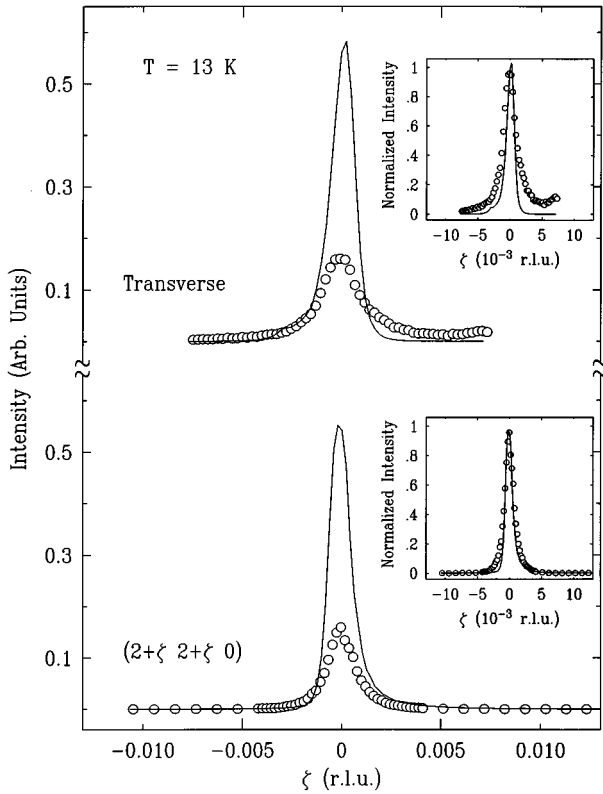


FIG. 5. Upper: Transverse scans through the $(2,2,0)$ chemical reflection taken on the mechanically roughened (open circles) and as-prepared (solid line) sides of the sample at 13 K. The scan direction is along $(0,0,1)$ in Fig. 1. Lower: Longitudinal scans through the $(2,2,0)$ chemical reflection on the mechanically roughened (open circles) and as-prepared (solid line) sides.

tation of diffracting crystallites, or a reduction in the average in-plane crystallite size (from 1300 to 800 Å), or both. These effects can usually be separated by characterizing the diffraction profile as a function of diffraction order. Unfortunately, with the long wavelengths required in these experiments to maintain the resonance condition, it is not possible to investigate the momentum-transfer dependence in this way. On the roughened side, the decrease in the integrated intensity, the increased mosaic width, and the additional scattering in the wings of the charge peaks are all consistent with significant structural damage and strain.

Important differences were also observed for the magnetic scattering, which is shown in Fig. 6. The upper and lower panels correspond to transverse and longitudinal scans taken through the magnetic $(1,1,0)$ peak at 13 K. Open circles represent data obtained on the mechanically roughened side of the sample, while solid lines represent that obtained on the as-prepared side. The corresponding counting rates were $\sim 50\,000$ and $\sim 200\,000$ /sec, respectively. In the inset, the amplitudes have again been scaled in order that the peak heights coincide. In contrast to the charge scattering, the magnetic profiles are considerably broadened in both the longitudinal and transverse directions.

On the roughened side, the longitudinal profile was fitted to a Lorentzian-squared line shape while the transverse profiles were fitted to Lorentzians. On the as-prepared side, the longitudinal profiles were fitted to Lorentzian-three-halves

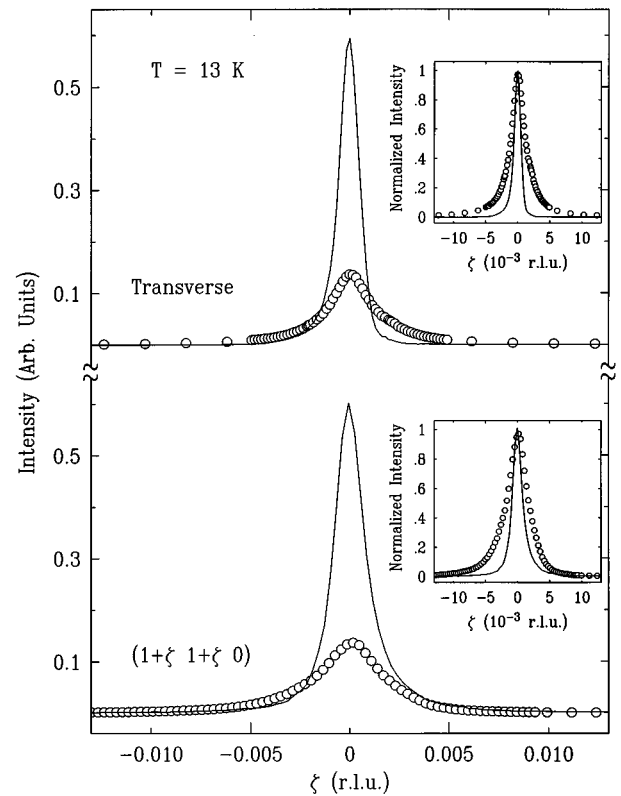


FIG. 6. Upper: Transverse scans through the $(1,1,0)$ magnetic reflection taken on the mechanically roughened (open circles) and as-prepared (solid line) sides of the sample in the magnetically ordered phase at 12 K. The scan direction is along the line with $\phi=68^\circ$ in Fig. 1. Lower: Longitudinal scans through the $(1,1,0)$ magnetic reflection on the mechanically roughened (open circles) and as-prepared (solid line) sides.

line shapes and the transverse profiles were fitted to Lorentzian-squared line shapes. The longitudinal full widths were found to be $0.0019\sqrt{2}a^* = 0.0031 \text{ \AA}^{-1}$ and $0.0036\sqrt{2}a^* = 0.0059 \text{ \AA}^{-1}$ on the as-prepared and roughened halves, respectively. The mosaic widths on the two sides were approximately 0.05° and 0.12° , respectively. The values obtained on the roughened side correspond to the averages taken from several different positions on the sample. By translating the sample across the beam variations of the mosaic width by as much as $\pm 20\%$ could be observed. Making the reasonable assumption that the longitudinal widths on the as-prepared side of the sample represent the resolution function at these scattering angles, we find magnetic correlation lengths along the surface normal direction of at least 650 Å on the as-prepared side and only 300 Å on the mechanically roughened side. It is clear that the damage present on the roughened side of the sample reduces the magnetic correlation lengths both in plane and along the surface-normal direction. Moreover, the magnetic correlation lengths are shorter than the lattice correlation lengths in both cases.

III. TEMPERATURE DEPENDENCE OF THE MAGNETIC SCATTERING

A. Order parameter

The temperature dependence of the magnetic scattering obtained by both x-ray and neutron scattering at the $(1,1,0)$

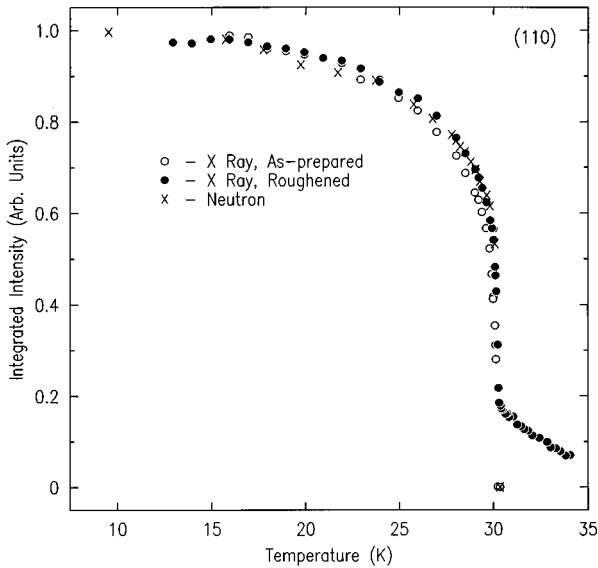


FIG. 7. Temperature dependence of the integrated magnetic intensities of the (1,1,0) reflection obtained by x-ray scattering on the as-prepared (open circles) and mechanically roughened (closed circles) sides of the sample. The same by neutron scattering (crosses).

reflection is shown in Fig. 7. These data were collected for temperatures increasing from 10 K, and were integrated at each temperature by rocking the sample. Open circles represent the results obtained by x-ray scattering from the as-prepared side; closed circles represent the x-ray-scattering results from the mechanically roughened side; and crosses represent the results obtained by neutron scattering from the whole sample. Since different cryostats were used in the x-ray- and neutron-scattering experiments the temperature scales have been adjusted by a few tenths of a kelvin to give the same value of T_N , namely, $T_N=30.2$ K. In addition, all the intensities have been scaled to be equal at 15 K, so that they can be directly compared. It is clear from the figure that for each data set there is an abrupt change near T_N and a saturation of the intensities below about 25 K, consistent with a first-order transition and with earlier neutron-scattering experiments.^{23–25} Thus the temperature dependences of the order parameter on the roughened and as-prepared sides appear identical to each other, and were very similar to the results of neutron-scattering experiments from the bulk. (The magnitude of the discontinuity exhibited by the neutron-scattering results appears larger than that obtained by x-ray scattering.) What is strikingly different among the three data sets is the appearance above T_N of additional, weak scattering on the mechanically roughened side of the sample (obtained by x-ray scattering) with a nearly linear dependence on temperature.

We have also characterized the temperature dependence of the magnetic intensity of the (2,1,0) reflection (see Fig. 1). These results are compared to those obtained for the (1,1,0) reflection for increasing temperatures in Figs. 8(a) and 8(b) for both the mechanically roughened and as-prepared sides of the sample, respectively. The qualitative behaviors observed at the two reflections are very similar, although the scattering was 20–30 % weaker at the (2,1,0) reflection. Additional scattering was again observed for the (2,1,0) reflec-

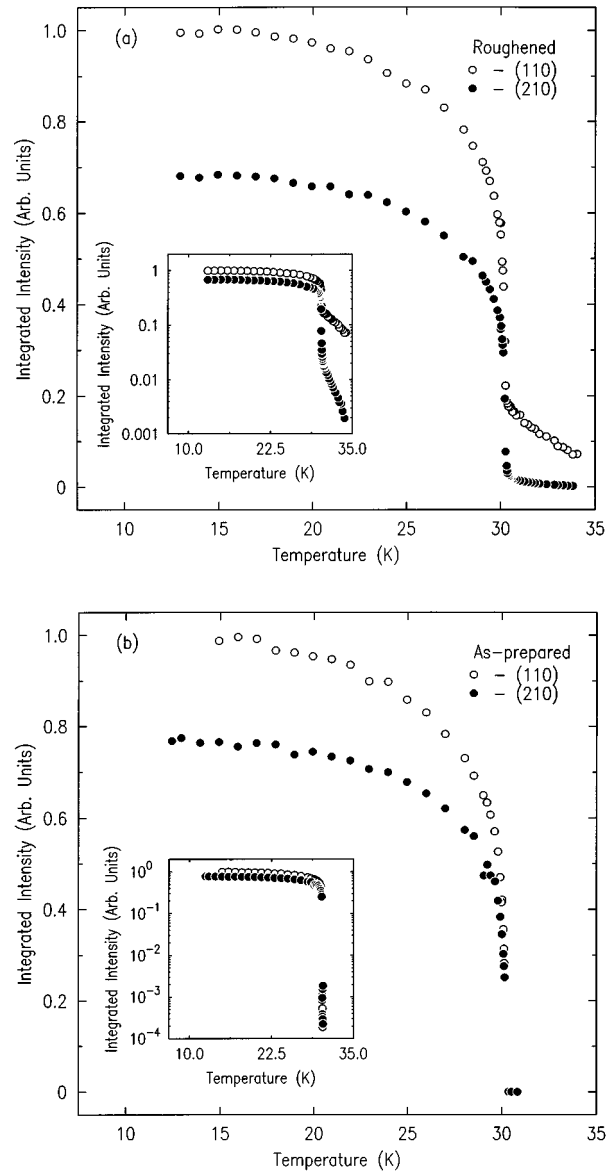


FIG. 8. (a) Temperature dependencies of the integrated magnetic intensities of the (1,1,0) and (2,1,0) reflections (open and closed circles, respectively) obtained on the mechanically roughened side of the sample. Inset: The same on a logarithmic scale. (b) The same as in (a), but obtained on the as-prepared side.

tion on the roughened side as much as 5 K above T_N [see inset, Fig. 8(a)]. The existence of additional scattering is similar to that which is observed for the (1,1,0) reflection, although it is about ten times weaker above T_N at the (2,1,0) reflection, and, as will be shown, it possesses a different temperature dependence of its peak position. No hysteresis was observed in the transition temperature for increasing and decreasing temperatures for either reflection, consistent with earlier neutron-scattering experiments.^{23–25}

To determine whether the additional scattering above T_N is indeed magnetic, we measured its dependence on incident x-ray energy at the (1,1,0) reflection as the energy was tuned through the M_{IV} absorption edge. The closed circles in Fig. 9 represent the scattering obtained in the ordered phase at a temperature of 15 K, while the open circles represent the additional scattering obtained at a temperature of $T_N+0.6$ K.

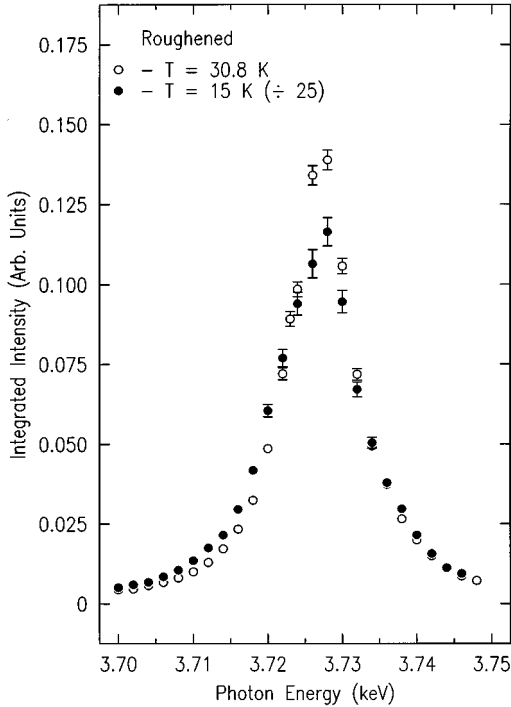


FIG. 9. Integrated magnetic intensity plotted versus incident photon energy of the (1,1,0) reflection at 15 K (closed circles) in the magnetically ordered phase and at $T_N+0.6$ K (open circles) in the critical regime.

The latter has been scaled by a factor of 25. The line shapes obtained at the two temperatures are identical to within statistics, and very similar to the line shapes obtained in earlier studies of the resonant magnetic scattering in UO_2 (Ref. 20)—very strong evidence that the additional scattering observed above T_N is magnetic.

B. Magnetic scattering above T_N

Figures 10 and 11 show representative transverse and longitudinal scans, respectively, of the additional magnetic scattering observed at the (1,1,0) reflection by x-ray scattering, for temperatures above $T_N=30.2$ K. Similar scans taken through the magnetic peak in the ordered phase at $T=12.9$ K are shown in the inset of each figure. They are plotted on identically scaled x axes to facilitate comparison. Referring to Fig. 10, it is clear that the additional scattering broadens in the transverse direction, and weakens, for temperatures increasing above T_N . After deconvolution from the resolution function, these line shapes are approximately described by Lorentzians.

The corresponding longitudinal scans are plotted versus temperature in Fig. 11. Just as occurs in the transverse direction, the peak broadens in the longitudinal direction, and weakens, for temperatures increasing above T_N . Also evident from Fig. 11 is an apparent shift in the position of the peak toward smaller h (and k). It should be emphasized that this shift does not correspond to a decrease in magnitude of the magnetic wave vector with temperature. In the conventional magnetic unit cell for UO_2 , the magnetic wave vector lies along the $[0,0,1]$ direction (within the surface plane), whereas the shift is measured along the surface-normal di-

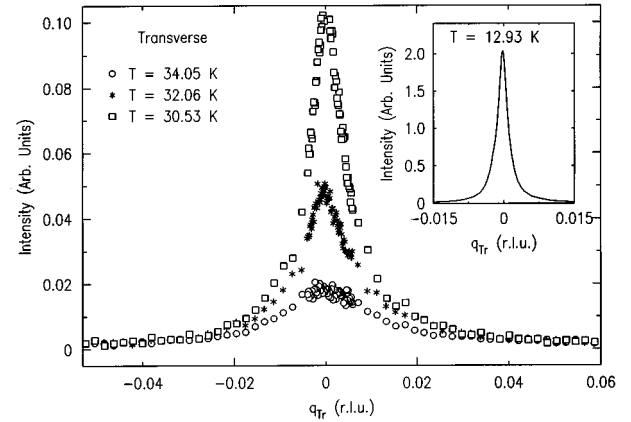


FIG. 10. Transverse scans taken along the $[0,0,1]$ direction through the (1,1,0) magnetic reflection versus temperature above $T_N=30.2$ K. Inset: Transverse scan through the (1,1,0) reflection in the ordered magnetic phase below T_N , for comparison.

rection. If the observed shift corresponded to a commensurate-incommensurate transition, similar to that which has been reported in studies of Tb (Refs. 10 and 11) and NpAs (Ref. 12) above T_N , then it would occur along the $[0,0,1]$ direction, and possess symmetry-related satellites located at $\pm q$ from the charge scattering. Similarly, if the observed shift corresponded to a small rotation of the magnetic wave vector, satellite pairs would occur along the $[1,1,0]$ direction. No additional satellites were observed in scans either longitudinal or transverse to the magnetic peak. Despite the small asymmetry evident toward smaller h , these line shapes are satisfactorily described by squared Lorentzians, after deconvolution of the resolution function.

The detailed temperature dependence of the longitudinal and transverse half-widths of the magnetic scattering from the mechanically roughened surface is shown on an absolute scale in Fig. 12(a). In the magnetically ordered phase, the longitudinal half-width is approximately 0.003 \AA^{-1} and the transverse half-width is 0.0014 \AA^{-1} . These correspond to correlation lengths of about 300 \AA along the surface-normal direction and 700 \AA within the surface plane. At T_N , both half-widths appear to increase discontinuously, and continue

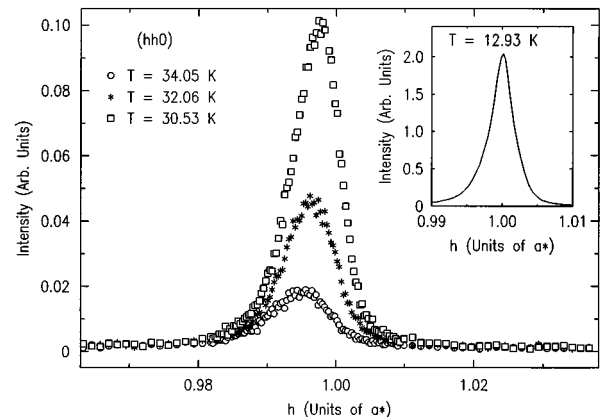


FIG. 11. Longitudinal scans taken through the (1,1,0) magnetic reflection versus temperature above T_N . Inset: Longitudinal scan taken through the (1,1,0) reflection in the ordered magnetic phase below T_N , for comparison.

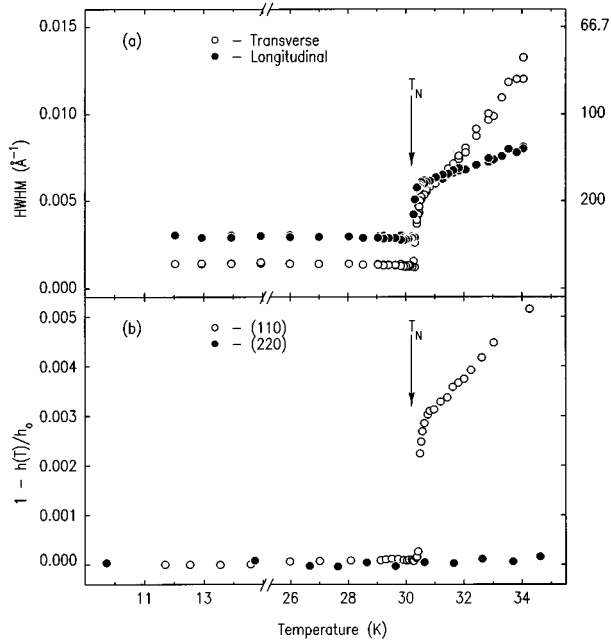


FIG. 12. (a) Temperature dependence of the longitudinal (closed circles) and transverse half-widths (open circles) of the (1,1,0) reflection after deconvolution of the resolution function. The transverse widths were obtained from rocking curves taken with $\phi=68^\circ$ in Fig. 1. (b) Position dependence of the magnetic scattering at the (1,1,0) reflection (open circles) measured along the (1,1,0) direction for temperatures increasing from 10 K. Closed circles show the corresponding behavior for the charge scattering at the (2,2,0) reflection.

increasing approximately linearly for temperatures above T_N . The shortest correlation lengths observed in these experiments were about 80 and 125 Å each in the transverse and longitudinal directions, respectively. This is comparable to within a factor of 2 to the shortest correlation lengths observed for the second length scale in Ho (Refs. 8 and 9) and Tb.^{10,11} However, in contrast to Ho and Tb, the scattering in UO₂ appears weakly anisotropic above T_N .

The position dependence of the magnetic scattering at the (1,1,0) reflection measured along the [1,1,0] direction is shown in Fig. 12(b) as a function of temperature. The measured d spacing in the (1,1,0) direction at each temperature is normalized by the d spacing obtained at 13 K: $1 - h(T)/h(13 \text{ K})$. Open circles represent the normalized position of the (1,1,0) magnetic reflection and closed circles represent the position of the (2,2,0) charge reflection. Below T_N , the positions of both the charge and magnetic peaks are constant. At T_N , there is an apparent jump in the position of the magnetic scattering by about 0.2% relative to the charge scattering, and a continuous, approximately linear, increase for temperatures increasing thereafter. This behavior mirrors the temperature dependence of the widths shown in Fig. 12(a). A similar jump is not seen in the temperature dependence of the lattice (shown by the filled circles) on either side of the sample.

Figure 13(a) shows the detailed temperature dependence of the longitudinal half-width of the additional magnetic scattering from the mechanically roughened side of the sample at the (2,1,0) reflection. The qualitative behavior is very similar to that obtained at the (1,1,0) reflection, includ-

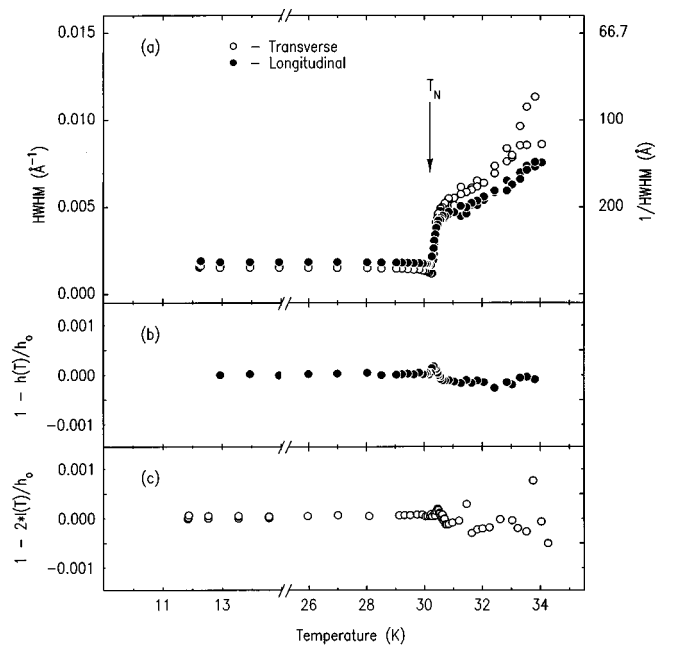


FIG. 13. (a) Temperature dependence of the longitudinal and transverse half-widths of the (2,1,0) reflection. Position dependence of the magnetic scattering in the longitudinal (b) and transverse (c) directions.

ing an apparent discontinuity at T_N and a linear increase above T_N . The temperature dependence of the peak position measured in two orthogonal directions around the (2,1,0) reflection is shown in Fig. 13(b). In contrast to the results obtained for the (1,1,0) reflection, no shift in position is observed above T_N .

It should be made clear that the data shown in Figs. 12 and 13 do not establish the existence of a discontinuity in the temperature dependence of the width or position of the additional magnetic scattering at T_N , nor do they necessarily imply a divergence of the magnetic correlation length at T_N . Recall that there is also an abrupt increase in intensity of the ordered phase magnetic scattering at the transition. This scattering entirely masks the behavior of the additional component, if it exists, below T_N . It is possible, therefore, that the widths and position of the additional component decrease continuously to lower temperatures. It should also be noted that, just as for the magnetic intensities obtained in the ordered phase, the absolute widths and amplitudes of the additional component at a given temperature are sample-position dependent. For this reason, we have not attached particular significance to the Lorentzian and squared-Lorentzian forms used in the fitting of the line shapes.

C. Comparison to neutron scattering

Elastic-neutron-scattering experiments were performed at the (1,1,0) reflection above T_N on both the roughened and as-prepared sides of the sample for comparison to the x-ray-scattering results. Short-ranged magnetic correlations consistent with earlier neutron-scattering results²⁷ were observed on both sides of the sample. Longitudinal and transverse scans of the (1,1,0) reflection obtained at $T = T_N + 0.9 \text{ K}$ are shown on the left-hand sides of Figs. 14 and 15, respectively. The solid lines through these data represent fits to Lorentzian

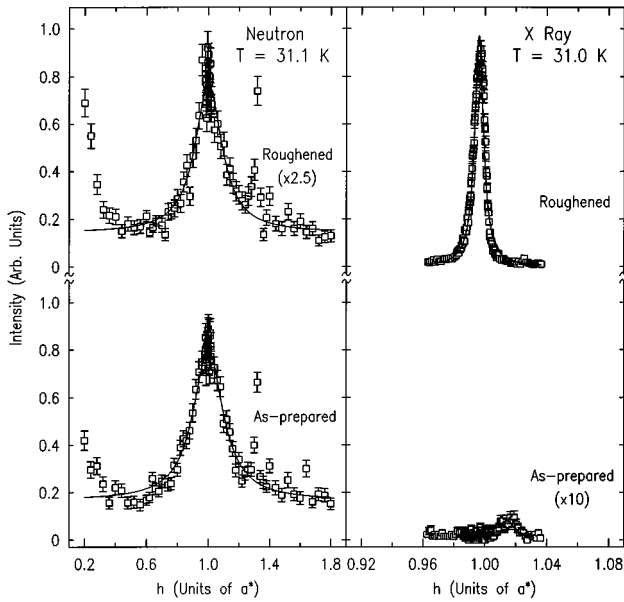


FIG. 14. Radial scans taken along the $[1,1,0]$ direction through the $(1,1,0)$ magnetic reflection on the mechanically roughened and as-prepared sides of the sample by neutron and x-ray diffraction. These scans were taken at a temperature about 1 K above T_N .

line shapes. (They are so broad that deconvolution of the resolution function was not necessary.) The neutron-scattering results obtained on both sides of the sample are identical. This is in contrast to the results of the x-ray-scattering experiments, which showed additional sharper scattering on the mechanically roughened side, but not on the as-prepared side. The corresponding scans obtained by x-ray scattering at similar temperatures are shown on the right-hand side, and have been fitted as discussed earlier in the text. It is important to note that the x -axis scale shown for the x-ray-scattering results is ten times narrower than that shown for the neutron-scattering results. Thus, the corresponding correlation lengths of the scattering probed by the two techniques differ by nearly a factor of 10, and suggest that different components of the magnetic scattering are measured by the two techniques.

The temperature dependence of the full widths of the magnetic fluctuations observed above T_N by neutron scattering in both the longitudinal and transverse directions is plotted in Fig. 16. Filled circles represent the data obtained on the as-prepared side of the sample, whereas filled squares represent the results obtained on the roughened side. It is clear from the figure that the widths increase approximately linearly above T_N . The absolute values are approximately ten times larger than observed by x-ray scattering at the same temperatures (see Fig. 12). There is no significant difference in comparing the two sides of the sample. These results are essentially identical to those reported by Buyers and Holden²⁷ on a different sample, and reproduced by the open squares in Fig. 16.

Long-counting x-ray-scattering experiments were performed on both sides of the sample and over the same regions of reciprocal space as probed in the neutron-scattering experiments in order to search for a broad component of the scattering. Similar long-counting scans were performed by

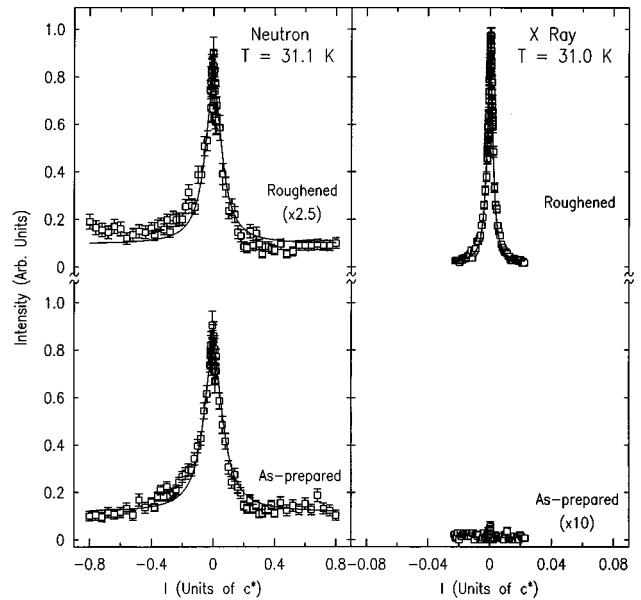


FIG. 15. Transverse scans taken along the $[0,0,1]$ direction through the $(1,1,0)$ magnetic reflection on the mechanically roughened and as-prepared sides of the sample by neutron and x-ray diffraction. These scans were obtained at a temperature about 1 K above T_N .

neutron scattering searching for the sharp component observed in the x-ray-scattering experiments. Neither were successful.

D. Azimuthal dependence

An interesting result which became evident during the course of these experiments was the observation of a strong dependence of the magnetic intensity on the azimuthal orientation of the sample with respect to the $(1,1,0)$ direction. Specifically, for $\phi=68^\circ$ (see Fig. 1), large counting rates of order 200 000/sec were observed at the $(1,1,0)$ reflection at 13 K on the as-prepared side, as noted above. However, when the sample was rotated about the $(1,1,0)$ axis to bring the $(1,0,0)$ reflection into the diffraction plane ($\phi=0$), the intensity dropped by more than a factor of 10. Since the polarization dependence of the x-ray magnetic cross section in dipole approximation depends simply on the direction of the magnetic moment (varying as $k' \cdot \hat{J}$ for a σ -polarized incident beam), this observation offers a means to determine the direction of the magnetic moment in UO_2 by measuring the azimuthal dependence of the magnetic intensity. Systematic studies with both $(1,1,0)$ - and $(0,0,1)$ -oriented samples are planned.

IV. DISCUSSION AND CONCLUSIONS

We summarize our results so far. The charge-scattering peaks which characterize the chemical reciprocal lattice of the mechanically roughened surface exhibit weaker integrated intensities, broader mosaic widths, and additional scattering in the wings around each reciprocal lattice point than the corresponding peaks on the as-prepared side. This is consistent with significant structural damage localized within about $\frac{1}{2} \mu\text{m}$ of the surface and implies an increased, probably

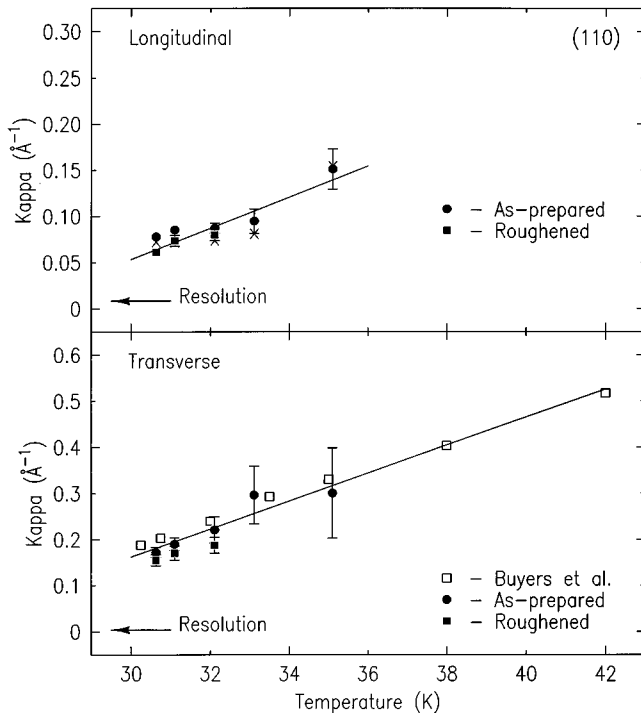


FIG. 16. The temperature dependence of the HWHM (K) of the transverse (upper) and longitudinal (lower) scans on the mechanically roughened (closed squares) and as-prepared sides (closed circles) of the sample obtained by neutron scattering. Open squares show the neutron-scattering results reported by Buyers and Holden (Ref. 25) on a different sample.

random, strain distribution. In particular, the additional scattering in the wings of the charge peaks suggests the existence of domains with lattice constants distorted about the bulk value.

The symmetries of the magnetic diffraction patterns obtained below T_N on the as-prepared and roughened sides of the sample are identical with each other and with the results of neutron diffraction. Similarly, the temperature dependences of the integrated magnetic intensities are mutually self-consistent below T_N . The line shapes of the magnetic scattering, however, are uniformly broader in both the transverse and longitudinal directions on the mechanically roughened side, leading to average magnetic correlation lengths of only 300 Å. In contrast, the longitudinal correlation lengths on the as-prepared side are at least ~ 650 Å. These should be compared with typical lattice correlation lengths of at least ~ 1000 Å on the as-prepared side, and with the $(1/e)$ x-ray-absorption length of about 1200 Å. Normal, short-ranged fluctuations were observed by neutron diffraction above T_N on both sides of the sample, but could not be observed by x-ray scattering.

The principal difference in the magnetic diffraction patterns of the roughened and as-prepared sides concerns the presence of weak scattering above T_N on the roughened side. This scattering exists both at the $(1,1,0)$ and $(2,1,0)$ reflections, although it is an order of magnitude weaker for the latter. It broadens continuously above T_N , and persists to temperatures as high as $T_N + 10$ K. Remarkably, the scattering at the $(1,1,0)$ reflection appears to shift along the $[1,1,0]$ direction with increasing temperature. This shift occurs along

the surface-normal direction and is perpendicular to the planes containing the moments. However, no shift is observed at the $(2,1,0)$ reflection. The behavior of the additional scattering below T_N , if it exists, could not be resolved.

It seems natural to conclude from the present experiments that the additional magnetic component observed in UO_2 originates in the mechanically damaged volume of the sample, and is associated with the strain. The failure of the neutron-scattering experiments to detect additional magnetic scattering reflects the small volume of the damaged region (compared to the large neutron penetration depth) and the low q resolution of the neutron-scattering experiments.⁹ Similarly, the ease with which the additional component was detected by x-ray scattering reflects the corresponding small $(1/e)$ absorption length and high q resolution used in the x-ray-scattering experiments. In this regard, the additional component is reminiscent of the second length scale observed among the critical magnetic fluctuations of Ho ,^{8,9} Tb ,^{10,11} and NpAs (Ref. 12) at their ordering transitions, and among the critical fluctuations of various perovskites¹⁻⁶ at their tetragonal-to-cubic structural transitions. It suggests that the second length scale originates from the strain, for example, which typically accompanies mechanical polishing of the sample surface prior to experiments.

We find this reasoning plausible. However, there are also important differences between our results for UO_2 and earlier results. First, the magnetic ordering transition in UO_2 is discontinuous, whereas all other examples are continuous or weakly first order. Also, the shift in position of the magnetic scattering at the $(1,1,0)$ reflection above T_N is unusual, and has not been reported in earlier investigations so far as we know.³⁹

An interesting interpretation for UO_2 is that the additional magnetic scattering remains commensurate with the lattice, but that the domains which support magnetic correlations are themselves distorted. Charge scattering from such particles has not been directly observed as a peak in reciprocal space; however, the wings of the bulk charge peaks are sufficiently broad as to include the positions of the distorted lattice. From this perspective, the additional magnetic scattering could arise from a distribution of finite-sized, strained particles. We can explain the apparent shift of the magnetic scattering with temperature if we further assume that T_N varies with the effective d spacing, with deformed regions with a larger $(1,1,0)$ d spacing possessing a higher T_N . A difficulty with this interpretation is the absence of a shift measured at the $(2,1,0)$ reflection. To explain the absence of a shift at $(2,1,0)$ may require proposing a second type of magnetic domain with magnetic wave vector along the $(0,1,0)$ direction. Distinguishing in this way among different types of domains, of course, breaks the assumption of a triple- Q magnetic structure in the distorted domains, but is perhaps consistent with the order of magnitude reduction in the intensities at the $(2,1,0)$ reflection compared with that at the $(1,1,0)$ reflection. Similar effects have been observed in the single- Q antiferromagnet UPd_2Al_3 .³⁹

It is worth noting a related interpretation which has been suggested by Bernhoeft *et al.*¹³ on the basis of x-ray resonant-magnetic-scattering studies of the additional magnetic component found above T_N in UAs and UP. Those

materials also possess discontinuous magnetic ordering transitions and simpler, single- Q magnetic structures. In contrast to the present results, they found strongly anisotropic magnetic scattering above T_N , which was interpreted in terms of “layer-by-layer” ordering in finite-sized blocks located near the surface. The extent to which detailed connections can be made to the present results for UO_2 will require further analysis of their ongoing experiments on UAs and UP.¹³

In the foregoing discussion, we have considered the possibility that the additional component corresponds to static magnetic order within finite-sized particles. It is also possible, indeed, most previous discussions of the two-length-scale problem have assumed, that the additional scattering arises from short-ranged, long-lived magnetic fluctuations. A suitable test which could distinguish these possibilities involves high-resolution, inelastic-neutron-scattering studies of the additional component. In principle, finite-sized domains supporting static magnetic order would give rise to purely elastic scattering, whereas critical fluctuations would give rise to quasielastic scattering. Experiments along these lines have been attempted in Tb (Ref. 11) and Ho,⁴⁰ where the additional component may be resolved at low scattering angles. No energy width beyond the resolution width of ~ 5 μeV has been established, setting a lower bound on the lifetime, but not resolving the question. Unfortunately, such experiments are outside present neutron-scattering capabilities for UO_2 .

It is interesting to note in this regard the recent calculations of Altarelli, Nunez-Regueiro, and Papoular⁴¹ in which the theory of critical phenomena in the presence of quenched disorder has been successfully applied to the two-length-scale problem for second-order transitions. In particular they have shown that long-range, random strains near a sample surface can induce crossover to a “disordered” fixed point with different critical exponents. Within the context of a particular model of the strain, they are able to reproduce elements of the experimental results obtained earlier for Ho and Tb.

To conclude, we have found that additional magnetic scattering is induced above T_N in UO_2 when its (1,1,0) surface is

mechanically roughened. Qualitative features of the scattering, including a typical length scale of about 100 Å and continuous broadening above T_N , are reminiscent of the two-length-scale problem discussed for Ho,^{8,9} Tb,^{10,11} and NpAs (Ref. 12) at their magnetic ordering transitions and in various perovskites¹⁻⁷ at their tetragonal-to-cubic structural transitions. From this perspective, our results suggest that the second length scale originates in the random strain fields which typically reside in the near-surface layers of samples whose surfaces are mechanically or chemically polished. That is the main result of our paper. Recent neutron-scattering studies of thin Ho films have also revealed two length scales above T_N .⁴² In that case, the necessary strain fields are likely correlated with the lattice mismatch at the substrate/film interfaces. (In our view, any source of random strains could induce a second length scale.) It has not been possible in any studies performed so far to prove whether the additional scattering arises from true, possibly long-lived, fluctuations or corresponds instead to static magnetic order within finite-sized, strained domains. It is crucial to find a system in which the strain can be continuously tuned, in order to quantitatively probe the physical origin of the second length scale.

ACKNOWLEDGMENTS

We acknowledge helpful discussions with J. D. Axe, N. Bernhoeft, M. Blume, P. Gehring, G. Helgesen, J. P. Hill, K. Hirota, S. Langridge, K. Lynn, S. G. J. Mochrie, G. Shirane, A. Stunault, and C. Vettier. We thank J. Rebizant and V. Meyritz for help in preparing the crystal. Work performed at Brookhaven was supported by the U.S. DOE under Contract No. DE-AC02-CH7600016. B.D.G. acknowledges financial support from NSERC of Canada, OCMR of Ontario, and the Alfred P. Sloan Foundation. Topography carried out at the Stony Brook Synchrotron Topography Station, Beamline X-19C, at the NSLS, BNL, was supported by DOE. Research was supported in part by the U.S. Army Research Office under Grants No. DAAH04-94-G-0091 and No. DAAH04-94-G-0121.

*Current address: University of Western Ontario, London, Ontario, Canada N6A 3K7.

¹S. R. Andrews, *J. Phys. C* **19**, 3721 (1986).

²T. W. Ryan, R. J. Nelmes, R. A. Cowley, and A. Gibaud, *Phys. Rev. Lett.* **56**, 2704 (1986).

³D. F. McMorro, N. Hamaya, S. Shimomura, Y. Fujii, S. Kishimoto, and H. Iwasaki, *Solid State Commun.* **76**, 443 (1990).

⁴A. Gibaud, T. W. Ryan, and R. J. Nelmes, *J. Phys. C* **20**, 3833 (1987).

⁵A. Gibaud, R. A. Cowley, and P. W. Mitchell, *J. Phys. C* **20**, 3849 (1987).

⁶U. J. Nicholls and R. J. Cowley, *J. Phys. C* **20**, 3417 (1987).

⁷Y. Imry and M. Wortis, *Phys. Rev. B* **19**, 3580 (1978).

⁸T. R. Thurston, G. Helgesen, D. Gibbs, J. P. Hill, B. D. Gaulin, and G. Shirane, *Phys. Rev. Lett.* **70**, 3151 (1993).

⁹T. R. Thurston, G. Helgesen, J. P. Hill, D. Gibbs, B. D. Gaulin, and P. J. Simpson, *Phys. Rev. B* **49**, 15 730 (1994).

¹⁰P. M. Gehring, K. Hirota, C. F. Majkrzak, and G. Shirane, *Phys. Rev. Lett.* **71**, 1087 (1993).

¹¹K. Hirota, G. Shirane, P. M. Gehring, and C. F. Majkrzak, *Phys. Rev. B* **49**, 11 967 (1994).

¹²S. Langridge, W. G. Stirling, G. H. Lander, J. Rebizant, J. C. Spirlet, D. Gibbs, and O. Vogt, *Europhys. Lett.* **25**, 137 (1994); S. Langridge, W. G. Stirling, G. H. Lander, and J. Rebizant, *Phys. Rev. B* **49**, 12 022 (1994).

¹³N. Bernhoeft, A. Stunault, C. Vettier, F. de Bergevin, D. Gibbs, T. R. Thurston, S. M. Shapiro, J. B. Hastings, P. Dalmas, G. Helgesen, and O. Vogt, in *Proceedings of ICM-94* [J. Magn. Magn. Mater.] **1421**, 140 (1995).

¹⁴J. D. Axe (private communication).

¹⁵See, for example, G. Grubel, K. G. Huang, D. Gibbs, D. M. Zehner, A. R. Sandy, and S. G. J. Mochrie, *Phys. Rev. B* **48**, 18 119 (1993).

¹⁶T. C. Lubensky and M. H. Rubin, *Phys. Rev. B* **12**, 3885 (1975); K. Binder, in *Phase Transitions and Critical Phenomena*, edited by C. Domb and J. L. Lebowitz (Academic, London, 1983), Vol. 8, p. 2; H. W. Diehl, *ibid.*, Vol. 10, p. 76; H. Dosch, *Critical Phenomena at Surfaces and Interfaces* (Springer-Verlag, Berlin, 1992).

- ¹⁷D. P. Osterman, K. Mohanty, and J. D. Axe, *J. Phys. C* **21**, 2635 (1988).
- ¹⁸R. A. Cowley (private communication).
- ¹⁹K. Hirota, J. P. Hill, S. M. Shapiro, G. Shirane, and Y. Fujii, *Phys. Rev. B* **52**, 13 195 (1995).
- ²⁰C. C. Tang, W. G. Stirling, G. H. Lander, D. Gibbs, W. Herzog, P. Carra, B. T. Thole, K. Mattenberger, and O. Vogt, *Phys. Rev. B* **46**, 5287 (1992).
- ²¹T. Nattermann and J. Villain, *Phase Transitions* **11**, 5 (1988).
- ²²D. Belanger, *Phase Transitions* **11**, 53 (1988).
- ²³B. C. Frazer, G. Shirane, D. E. Cox, and C. E. Olsen, *Phys. Rev.* **140**, A1448 (1965); B. T. M. Willis and R. I. Taylor, *Phys. Lett.* **17**, 188 (1965). Note that T_N is given in this paper as 30.8 K. Allowing for differences in thermometry, the two measurements are consistent.
- ²⁴J. Faber and G. H. Lander, *Phys. Rev.* **14**, 1151 (1976).
- ²⁵J. Rossat-Mignod, G. H. Lander, and P. Burlet, in *Handbook of the Physics and Chemistry of the Actinides*, edited by A. J. Freeman and G. H. Lander (Elsevier, Amsterdam, 1984), Vol. 1, p. 415.
- ²⁶O. G. Brandt and C. T. Walker, *Phys. Rev.* **170**, 528 (1968).
- ²⁷W. J. L. Buyers and T. M. Holden, in *Handbook of the Physics and Chemistry of the Actinides*, edited by A. J. Freeman and G. H. Lander (Elsevier, Amsterdam, 1985), Vol. 2, p. 239.
- ²⁸D. Gibbs, D. R. Harshman, E. D. Isaacs, D. B. McWhan, D. Mills, and C. Vettier, *Phys. Rev. Lett.* **61**, 1241 (1988).
- ²⁹D. Gibbs, G. Grubel, D. R. Harshman, E. D. Isaacs, D. B. McWhan, D. Mills, and C. Vettier, *Phys. Rev. B* **43**, 5663 (1991).
- ³⁰J. P. Hannon, G. T. Trammell, M. Blume, and D. Gibbs, *Phys. Rev. Lett.* **61**, 1245 (1988).
- ³¹D. B. McWhan, C. Vettier, E. D. Isaacs, G. E. Ice, D. P. Siddons, J. B. Hastings, C. Peters, and O. Vogt, *Phys. Rev. B* **46**, 5287 (1992).
- ³²J. Luo, G. Trammell, and J. P. Hannon, *Phys. Rev. Lett.* **71**, 287 (1993).
- ³³P. Carra and B. T. Thole, *Colloq. Rev. Mod. Phys.* **66**, 1509 (1994).
- ³⁴M. Blume, in *Proceedings of the 2nd International Conference on Research Anom. X-Ray Scattering, Hamburg, 1993*, edited by G. Materlick, C. J. Sparks, and K. Fisher (Elsevier, Amsterdam, 1994).
- ³⁵G. Helgesen, J. P. Hill, T. R. Thurston, and D. Gibbs, *Phys. Rev. B* **52**, 9446 (1995).
- ³⁶Hj. Matzke and A. Thuros, *J. Nucl. Mater.* **114**, 349 (1983).
- ³⁷Hj. Matzke, *Phys. Status Solidi A* **8**, 99 (1971).
- ³⁸P. J. Schultz and K. G. Lynn, *Rev. Mod. Phys.* **60**, 701 (1988).
- ³⁹M. Mao, M. Lumsden, L. Taillefer, and B. D. Gaulin (unpublished).
- ⁴⁰T. R. Thurston, J. P. Hill, G. Helgesen, D. Gibbs, J. Borchers, and R. Erwin (unpublished).
- ⁴¹M. Altarelli, M. D. Nunez-Regueiro, and M. Papoular, *Phys. Rev. Lett.* **74**, 3840 (1995).
- ⁴²P. Gehring, A. Vigliante, D. McMorrow, D. Gibbs, C. F. Majkrzak, G. Helgesen, R. A. Cowley, R. C. C. Ward, and M. R. Wells, *Physica A* (to be published).